Baroclinic Rossby waves as inferred from temperature fluctuations in the Eastern Pacific

by William J. Emery[1,2] and Lorenz Magaard[1]

ABSTRACT

Monthly mean values of temperature from both hydrographic and XBT casts are used to compute isotherm displacements at weather station November (30N, 140W) and at six 2-degree squares between Hawaii and the weather station. A composite spectrum computed from all the isotherms in the six 2-degree squares shows significantly higher potential energy in the frequency range below the theoretical cut-off frequency (corresponding period about five months) for baroclinic Rossby waves. The first five baroclinic modes are computed from the mean density profile at station November, and these modes fit in the time domain to the isotherm displacements at the weather station. This fit indicated the predominance of the first mode.

Next, a cross-spectral fit of a Rossby wave model (random field of baroclinic waves) is made to the time series of isotherm fluctuations. At station November alone, a fit using the first four modes accounts for about 75% to 85% of the fluctuations at periods of about one to two years. This fit also indicates the predominance of the first mode, hence a cross-spectral fit using the first mode only is made to the isotherm fluctuations in the six 2-degree squares. This fit accounts for about 65% to 75% of the observed fluctuations at periods of about one to two years and indicates waves propagating in distinct directions between 20 and 80 degrees west of north with wavelengths between 1200 km and 1700 km. The group velocities of these waves are directed almost exactly westward and have magnitudes of about 4.5 cm s^{-1}. For smaller wave periods (about 5 to 9 months) the angular range of propagation directions widens to isotropic propagation in the western half plane.

1. Introduction

Monthly mean values of subsurface temperature, from the eastern Pacific, have been used in some recent studies (Bernstein and White, 1974; Emery, 1975). Their time series of mean temperature values appear to contain wave-like fluctuations. Therefore, we have begun to investigate the extent to which these fluctuations could be due to fields of known waves. From expendable bathythermograph (XBT) data, we have prepared time series of monthly mean values in the layer between 200 m and 500 m for six 2-degree squares in the region between Hawaii and weather

1. Department of Oceanography, University of Hawaii, Honolulu, Hawaii, 96822, U.S.A.
2. Current address: Department of Oceanography, Texas A. & M. University, College Station, Texas, 77843, U.S.A.

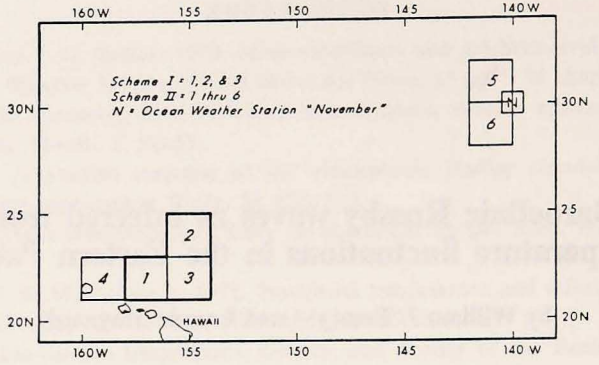

Figure 1. Locations of the six 2-degree squares and weather station November (N).

station November (30N, 140W). Hydrographic data from a 1-degree square around the weather station were used to form similar time series in the layer between 100 m and 3000 m.

These data provide a good opportunity to examine the possible existence of internal Rossby waves in the ocean. For this purpose, we first study the frequency and depth distribution of the fluctuations, arriving at a spectrum of potential energy for the upper layer of the ocean. These investigations strengthen our suspicion that Rossby waves could be partly responsible for the low-frequency portion of the observed fluctuations. We therefore develop a Rossby wave model which we then fit to the observations. This was done as a cross-spectral fit in extension of the work of Schott and Willebrand (1973) and Schott (1974) who applied a similar fit to internal gravity waves.

2. Data

The XBT observations used to form the time series in the six 2-degree squares were taken by ships of opportunity traveling between California and Hawaii. Under a program of the National Marine Fishery Service, XBT's have been taken along this route on a semimonthly basis since May, 1966. To these data were added other observations from the XBT file of Fleet Numerical Weather Central. The data were linearly interpolated for every 20 m of depth down to 500 m and the resulting temperatures were averaged within the month and 2-degree square in which they were taken. The period of best coverage was from May, 1966 to December, 1970 because of a large gap due to a shipping strike. The locations of the six squares chosen for this study are shown in Fig. 1.

The hydrographic data in the 1-degree square around the weather station were taken by ships occupying this weather station. A program of the U.S. Coast Guard (Husby, 1968), to study the oceanographic environment at station November, provided almost daily coverage of hydrographic data in the months from July, 1966

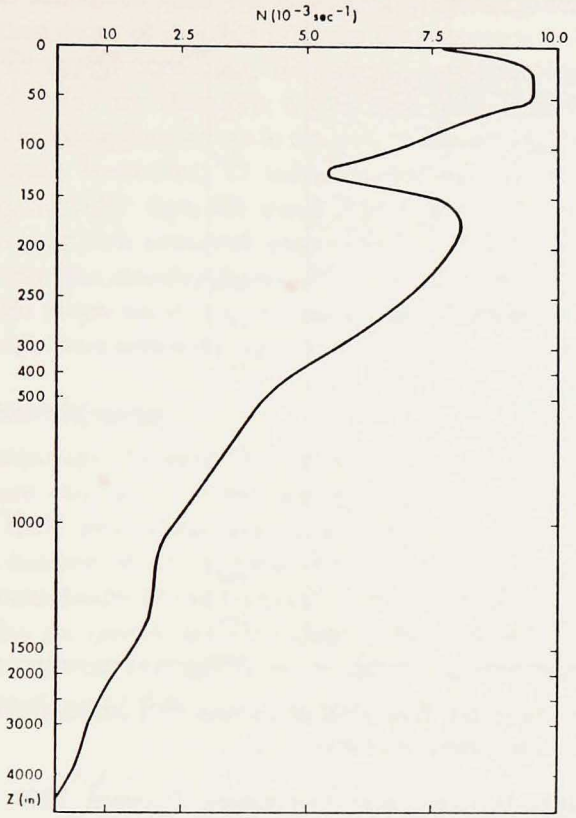

Figure 2. Vertical distribution of Brunt-Vaisala frequency at weather station November. (Note changes in vertical scale at 300 m and 1500 m).

to December, 1969. The temperature records from this station were linearly interpolated to give temperature values every 25 m between 0 m and 300 m, every 100 m between 300 m and 1500 m and every 500 m between 1500 m and 4500 m. The interpolated values were then averaged over the month in which they were taken to form a time series of temperature structure between the surface and 4500 m. The averages of these temperature values over the 42 months were used to calculate the mean profiles of potential density and the Brunt-Vaisala frequency (Fig. 2).

The number of observations used in the computation of the mean temperature values varied from month to month. Moreover, these observations were irregularly distributed in time and space. It was therefore a crucial question as to how good an estimate of the real monthly temperature means our values were. One solution to this question is to compare the change in monthly values to the amount of variation within a month. The standard error is a measure of this variation, therefore, the average standard error from adjacent monthly values was compared to the

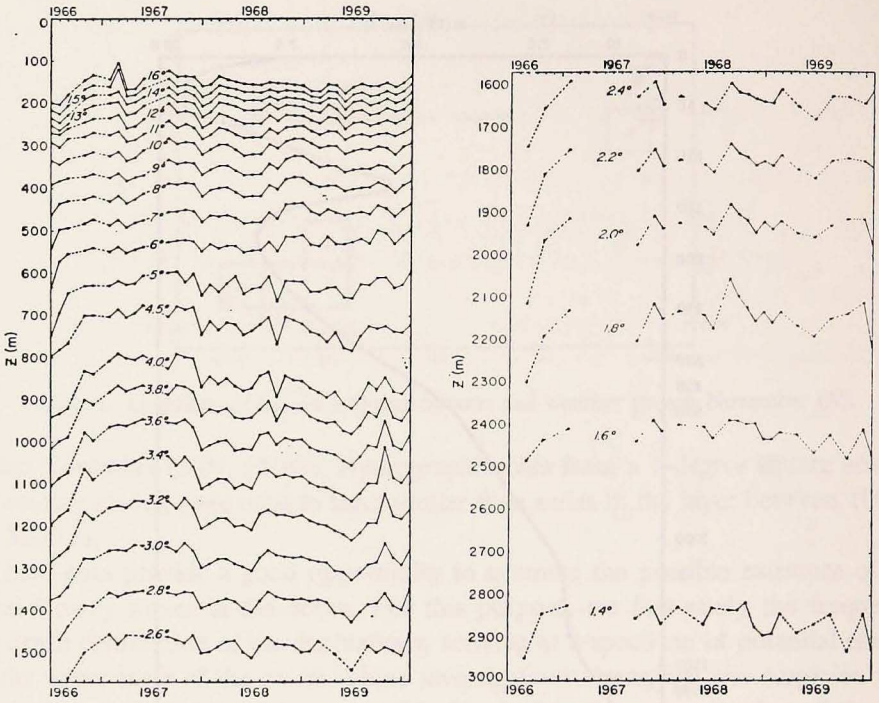

Figure 3a (left) and 3b (right). Time series of isotherm (°C) displacements at weather station November. Dotted lines: interpolated data.

temperature change between these two values. Between 70% and 90% of all changes were greater than the average standard error (see Table 1). About 50% to 80% of the changes were greater than the 95% confidence limits which corresponds approximately to twice the standard error. The high percentage of temperature changes greater than the standard error indicates that fluctuations with periods shorter than a month (such as internal tides) have small amplitudes in this region. Further evidence of the reliability of the monthly values will be given later (section 6) as a result of the cross-spectral fit.

In the 2-degree squares, the fluctuations of nine isotherms between 9°C and 17°C were chosen for study. The mean depths of these isotherms over the 56 month period were computed from the time series described above. These mean

Table 1. Percentage of reliable temperature changes.

	November	1	2	3	4	5	6
Greater than δ*	.64	.51	.48	.47	.65	.77	.59
95% Confidence level ($\approx 2\delta$)	.77	.75	.71	.70	.82	.87	.77

* δ = standard error.

depths were then subtracted from the monthly average depths of respective isotherms to form time series of monthly isotherm displacements ζ. In the region between Hawaii and station November, the selected isotherms were usually found between 150 m and 480 m. Therefore, the 54 time series computed from the six squares represent isotherm fluctuations in the layer between these depths.

At weather station November, 27 isotherms between 1.4°C and 16°C were selected. As with the XBT data, the mean depths of the chosen isotherms were computed for the complete period of observation. As before, these mean depths were subtracted from the monthly depths and 27 time series of ζ fluctuations were formed. These time series are shown in Figs. 3a and 3b where it can be seen that the chosen isotherms were within the layer between 150 m and 3000 m.

3. Spectrum of potential energy

In order to determine the important frequencies of the observed fluctuations, spectra $E_i(\omega)$ were computed for 49 time series of isotherm displacements $\zeta_i(t)$ calculated from XBT data. These spectra had only four degrees of freedom per spectral estimate because of the shortness of the time series. Assuming stationarity and horizontal homogeneity of the fluctuations, more significant spectra were produced by averaging the spectra, corresponding to the same depth interval, over the six squares. These spectra were multiplied by $N^2(z)$ and then integrated over z to form the spectrum of potential energy in the layer between 207 m and 367 m;

$$E_p(\omega) = \tfrac{1}{2}\,\rho_0 \int_{207m}^{367m} N^2(z) S(\omega,z)\,dz \tag{3.1}$$

where $S(\omega,z)$ are the spectra of ζ fluctuations averaged over the six squares, $N(z)$ is the Brunt-Vaisala frequency (z downward) and ζ_0 is a reference density. $E_p(\omega)$ is shown in Fig. 4.

In determining the effective degrees of freedom (K) for $E_p(\omega)$ we must realize that the 49 series are not independent. If they were completely independent K would be 196; if they were completely dependent K would be 4. According to Willebrand (J. Willebrand, personal communication) we can find K of a composite spectrum $E_p(\omega) = \sum_i \alpha_i E_i(\omega)$ from

$$K = \frac{\left(\sum_i \alpha_i E_i\right)^2 d}{\sum_{i,j} \alpha_i \alpha_j \gamma_{ij}^2 E_i E_j} \tag{3.2}$$

where γ_{ij} is the coherence between ζ_i and ζ_j and d is the number of degrees of freedom of the individual spectra $E_i(\omega)$. Applying (3.2) to our case (adjusting the α_i accordingly) we find $K \approx 10$. To obtain a larger K we have redone the calculation with $d = 8$. The resulting smoothed spectrum ($E_p(\omega)$) does not differ significantly from the one in Fig. 4 except that we no longer have a point at 28 months. In this

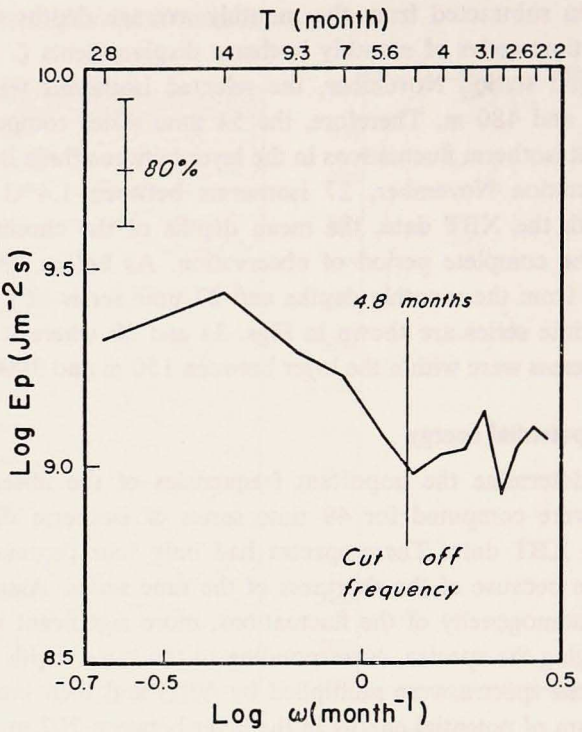

Figure 4. Spectrum of potential energy.

case we obtain $K \approx 25$ which leads to the 80% confidence limits displayed in Fig. 4.

This spectrum has two distinct energy levels, with the higher energy at low frequencies. The highest spectral peak is at a period of 14 months. The increase of spectral energy at low frequencies begins at a period of about five months which is close to the cut-off period (4.8 months, to be shown later) for baroclinic Rossby waves at 25N. This leads us to further investigate the possible wave character (baroclinic Rossby waves) of the fluctuations.

4. Vertical distribution of isotherm fluctuations (fitting in the time domain)

As a first step in determining the vertical distribution of the isotherm displacements, we computed the first five baroclinic Rossby wave modes. These modes are the solutions of the equation for the vertical velocity w:

$$\frac{d^2w}{dz^2} + \lambda^2 N^2 w = 0 \tag{4.1}$$

subject to the boundary conditions

$$w = 0 \text{ at } z = 0, H \ . \tag{4.2}$$

In these equations

$$\lambda^2 = \frac{\kappa\beta - \omega K^2{}_h}{\omega f^2} \tag{4.3}$$

H is the depth of the water, ω frequency of the wave, K_h horizontal wave number ($K^2{}_h = K^2 + \eta^2$), K and η wave numbers in the x and y direction (x to the west, y to the north), f the Coriolis parameter, and $\beta = df/dy$. Equations (4.1) and (4.2) are also valid for internal gravity waves where $\omega^2 << N^2$ and

$$\lambda^2 = \frac{K_h{}^2}{\omega^2 - f^2} \tag{4.4}$$

These modes can therefore also serve for possible investigations of long internal gravity waves (i.e. tides).

Equations (4.1) and (4.2) were solved for the first five modes by the "C-root method" described in Preisendorfer, *et al.* (1974). For this, we used $N(z)$ as computed at station November (Fig. 2) where the water depth (H) was 4755 m. The resulting eigenfunctions of vertical velocity were then normalized as

$$\phi_n(z) = \frac{W_n(z)}{(\int_0^H N^2(z) W^{\,2}{}_n(z)dz)^{\frac{1}{2}}} \tag{4.5}$$

where n indicates the mode number. These normalized eigenfunctions ($\phi_n{}^{(z)}$) are shown in Fig. 5. The corresponding eigenvalues (in $m^{-1}s$) are $\lambda_1 = 0.3343$, $\lambda_2 = 0.707$, $\lambda_3 = 1.091$, $\lambda_4 = 1.393$, and $\lambda_5 = 1.959$. According to (4.3) the dispersion relation for the nth mode is

$$\left(K - \frac{\beta}{2\omega}\right)^2 + \eta^2 = \frac{\beta^2}{4\omega^2} - f^2 \lambda^2{}_n \tag{4.6}$$

We consider λ_n and ϕ_n to be representative for the whole area under investigation and attach the β-plane at 25N. Hence the cut-off periods (in months), given by $T_n = 4\pi f \frac{\lambda_n}{\beta}$ are $T_1 = 4.8$, $T_2 = 10.2$, $T_3 = 15.7$, $T_4 = 20.1$, $T_5 = 28.2$.

The next step was to fit, in the time domain, the normalized eigenfunctions to the ζ fluctuations computed at weather station November. To do this, the coefficients $An(t)$ of the modes were chosen to minimize the expression

$$\int_0^H (\zeta(z,t) - \sum_{n=1}^{5} A_n(t)\, \phi_n(z))^2 dz \tag{4.7}$$

The resulting coefficients $A_n(t)$ are shown in Fig. 6 for the period July, 1966 to December, 1969. Also shown in the figure is the deviation

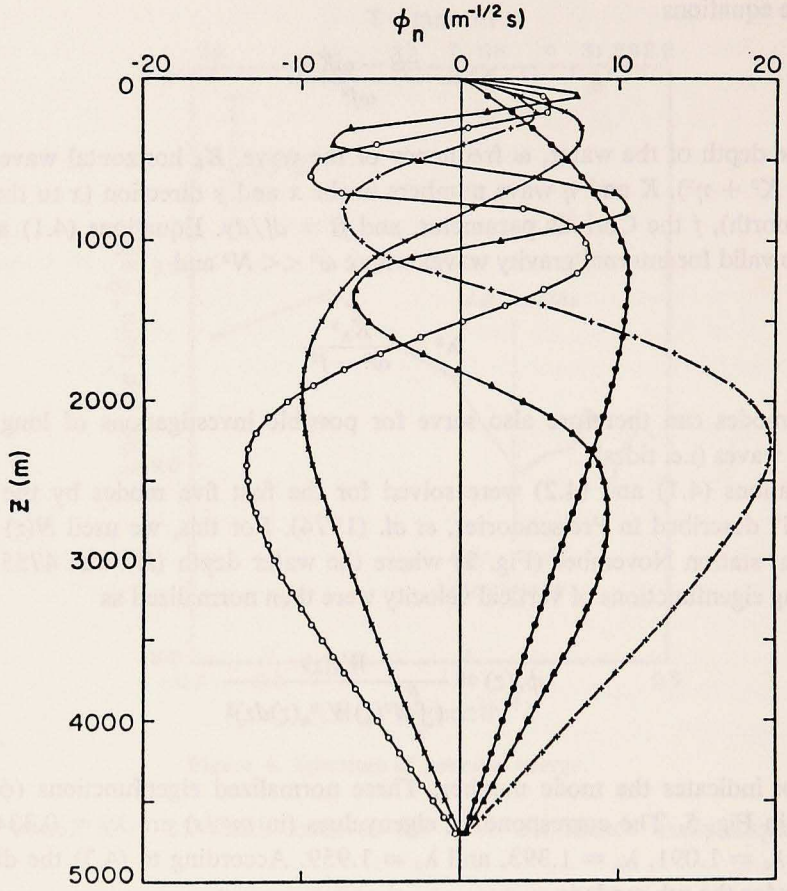

Figure 5. Normalized vertical velocity of the first five internal modes computed from the mean density profile at weather station November; (● = mode 1, x = mode 2, + = mode 3, ○ = mode 4, ▲ = mode 5).

$$D(t) = \frac{\int_0^H N^2(z)(\zeta(z,t) - \sum_{n=1}^{5} A_n(t)\phi_n(z))^2 dz}{\int_0^H N^2(z)\zeta^2(z,t)dz} \tag{4.8}$$

of the observed isotherm displacement from the modal fit. As can be seen in Fig. 6, the deviation is almost always less than 50% and is usually less than 25%. The mean deviation is 32%.

In this fit, the importance of the first mode can be clearly seen from the relatively large amplitude of A_1. It also appears that the lower frequency fluctuations have larger amplitudes. Both of these observations are confirmed by the spectral values computed from the time series in Fig. 6 (see Table 2). These spectral estimates,

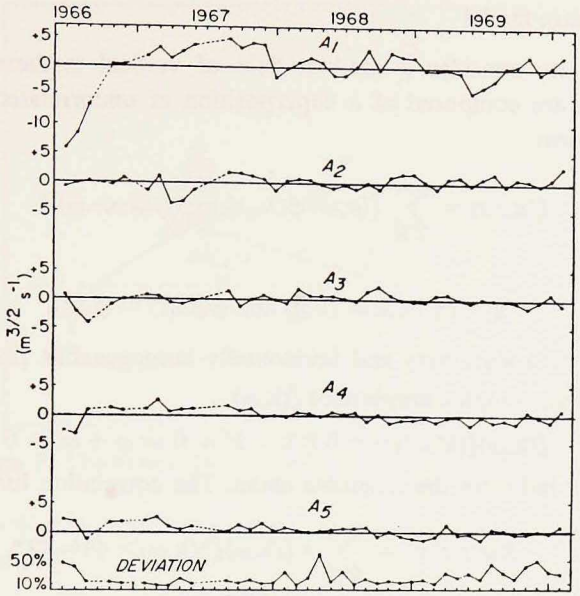

Figure 6. Coefficients (A_n (t)) of the first five internal modes as fit, in the time domain, to isotherm displacements at weather station November.

though not statistically significant, clearly show the highest spectral values at low frequencies for A_1. The higher modes have much smaller spectral values at all frequencies.

Our results are consistent with the idea that the observed fluctuations are mainly due to first mode baroclinic Rossby waves having periods greater than five months. The time series contain, of course, fluctuations of shorter periods. To obtain more conclusive results, we need to restrict our fit to the frequency range of the possible Rossby waves. One way to achieve this is to carry out a cross-spectral fit at the appropriate frequencies. Using this method, we can determine to what extent the vertical and horizontal structure of the observed field can be described by a Rossby wave model.

Table 2. Spectral values for A_1 through A_5 at periods between 5 and 22 months in m^3s^{-2}.

Period (months)	Coefficient of baroclinic mode				
	A_1	A_2	A_3	A_4	A_5
22	9.6	0.4	0.4	0.3	0.2
11	5.0	0.5	0.1	0.2	0.3
7.3	2.4	0.6	0.6	0.2	0.1
5.5	1.0	0.0	0.3	0.2	0.1

5. The Rossby wave model

In a β-plane, we consider a random field of vertical isotherm displacements ζ ($\mathbf{x}$, z, t) which are composed of a superposition of uncorrelated free baroclinic Rossby wave modes:

$$\zeta(\mathbf{x},z,t) = \sum_{\omega,\mathrm{K}} \xi(\mathbf{k},\omega)\, \phi(\lambda_n,z) \exp\,[i(\mathbf{k}\cdot\mathbf{x}-\omega t)] \tag{5.1}$$

where

$$\mathbf{x} = (x,y),\ \mathbf{k} = (k,\eta) \text{ and } \phi(\lambda_n,z) = \phi_n(z).$$

We assume ζ to be a stationary and horizontally homogeneous process. Hence we have for the random complex amplitudes $\xi(\mathbf{k},\omega)$

$$<\xi(\mathbf{k},\omega)\xi(\mathbf{k}',\omega')> = 0 \text{ if } \mathbf{k} + \mathbf{k}' \neq 0 \text{ or } \omega + \omega' \neq 0 \tag{5.2}$$

where $<\ldots\ldots>$ indicates the ensemble mean. The correlation function of ζ is

$$K(r,z,z',\tau) = \sum_{\mathrm{K},\omega} <\xi(\mathbf{k},\omega)\xi^*(\mathbf{k},\omega)>\, \phi(\lambda_n,z)\cdot$$
$$\phi(\lambda_n,z') \exp\,[-i(\mathbf{k}\cdot\mathbf{r}-\omega\tau)] \tag{5.3}$$

where $\mathbf{r} = \mathbf{x}' - \mathbf{x}$, $\tau = t' - t$ and * denotes the complex conjugate. Introducing a continuous representation,

$$<\xi(\mathbf{k},\omega)\xi'(\mathbf{k},\omega)> \cong E(\mathbf{k},\omega)d\mathbf{k}d\omega \tag{5.4}$$

and assuming that the wave field consists of modes up to the Mth order only,

$$E(\mathbf{k},\omega) = \sum_{n=1}^{M} \frac{E_n}{R_n} S_n(\phi)\delta(R-R_n) \tag{5.5}$$

we find the cross-spectrum to be

$$A(\mathbf{r},z,z'\omega) = \sum_{n=1}^{M} E_n\phi_n(z)\phi_n(z')e^{-i\,\frac{\beta}{2\omega}\,r\sin\alpha} +$$
$$\int_0^{2\pi} Sn(\phi) \exp\,\{-iR_n \cos\,(\phi-\alpha)\}\, d\phi. \tag{5.6}$$

Here r is the magnitude of $\mathbf{r}$ and α describes its direction (α positive from north to west) and $R^2{}_n = (\beta^2/4\omega^2 - f^2\lambda^2{}_n)$ (see 4.6) is the radius of the circle determined by the possible wave number vectors of the nth mode at frequency ω (Fig. 7). In Fig. 7, c_g points in the direction of the group velocity vector. Its magnitude is

$$C_g = \frac{2\omega^2 R_n}{\beta k}\ ; \tag{5.7}$$

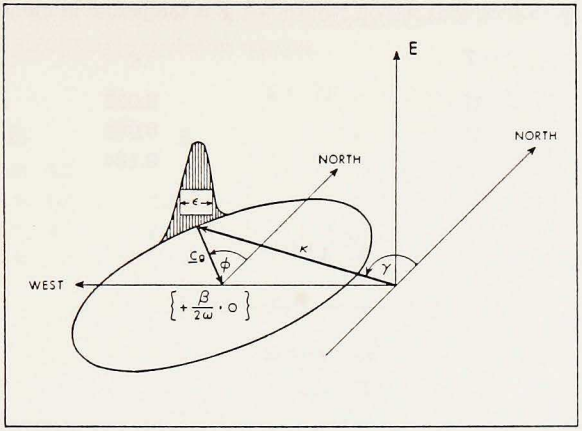

Figure 7. The circular locus of the wave numbers of the nth mode.

its direction is $\phi + \pi$. $S_n(\phi)$ is the directional distribution of $E(\mathbf{k},\omega)$ on this circle and is normalized as

$$\int_0^{2\pi} S_n(\phi)d\phi = 1 \ . \tag{5.8}$$

From (5.6) we find the co-spectrum C and the quadrature-spectrum Q according to $A = C - iQ$. One of the co-spectra, namely

$$C(0,z,z,\omega) = \sum_{n=1}^{M} E_n \phi^2{}_n(z) \tag{5.9}$$

is the auto-spectrum of ζ which explains the meaning of E_n as a measure for the energy of the nth mode.

6. Fitting the Rossby wave model to observations

In the case where observations from only one location are used the model can be applied without restriction. For a single location $r = 0$ and hence from (5.6)

$$A(0,z,z',\omega) = \sum_{n=1}^{M} E_n \phi_n(z)\phi_n(z') = C(0,z,z',\omega) \tag{6.1}$$

and

$$Q(0,z,z',\omega) = 0 \ . \tag{6.2}$$

These theoretical cross-spectra were fit to the cross-spectra computed from 21 time series of ζ at station November (Figs. 1 and 3a). Before fitting these spectra, however, the observed cross-spectra were checked for consistency with the model. According to (6.2), for the observations to be consistent with our model it is necessary that

Table 3. Consistency coefficient at station November. T is the period in months.

T	q
22	0.032
11	0.066
7.3	0.184

$$q = \frac{\sum_{s=1}^{S} Q_*^{(s)2}}{\sum_{s=1}^{S} C_*^{(s)2}} << 1 \tag{6.3}$$

where $C_*^{(s)}$ and $Q_*^{(s)}$ are the co- and quadrature-spectra computed from the series and s indicates the pair of S series ($s = 1, 2, \ldots, S$). For station November, $S = 231$.The values of q are given in Table 3 and show the data to be sufficiently consistent especially for the lower frequencies.

In light of these results the cross-spectra of (6.1) and (6.2) were then fit to the observed cross-spectra for $M = 1, 2, 3$ and 4. This least squares fit was accomplished by minimizing the function

$$F = \sum_{s=1}^{S} \{(C_*^{(s)} - C^{(s)})^2 + (Q_*^{(s)} - Q^{(s)})^2\} \tag{6.4}$$

where $C^{(s)}$ and $Q^{(s)}$ are the theoretical cross-spectra for the s pair. In this case where $r = 0$, we have from (6.1) and (6.4)

$$F(E_1, E_2, \ldots, E_m) = \sum_{s=1}^{S} [(C_*^{(s)} - \sum_{n=1}^{M} D_{ns} E_n)^2 + Q_*^{(s)2}] \tag{6.5}$$

where $D_{ns} = \phi_n(z_s)\phi_n(z'_s)$. To minimize F it is necessary that

$$\sum_{n=1}^{M} \left(\sum_{s=1}^{S} D_{ns} D_{ks} \right) E_n = \sum_{s=1}^{S} D_{ks} C_*^{(s)}; k = 1, 2, \ldots, M \ . \tag{6.6}$$

Equation (6.6) was used to find $E_1, E_2, \ldots, E_M$ for $M = 1, 2, 3$ and 4 at a period of 22 months, $M = 1, 2$ at 11 months, and $M = 1$ at 7.3 months. These are the maximum values of M allowed by the cut off periods of the various modes. The results are displayed in Table 4. Also in this table are values of F_{min}/F_0 which is a measure of the quality of the fit where

$$F_0 = \sum_{s=1}^{S} (C_*^{(s)2} + Q_*^{(s)2}) \tag{6.7}$$

If $F_{min}/F_0 = 0$ the fit is perfect; $F_{min}/F_0 = 100$ percent means that none of the observations are described by the model.

Table 4. Resulting E_n (m^3 month • s^{-2}) from cross-spectral fit at weather station November (with standard error). T is the period in months.

$T = 22$

M	E_1	E_2	E_3	E_4	F_{min}/F_0
1	19.9 ± 5.2				19.5%
2	19.9 ± 6.1	1.0 ± 0.0			19.4%
3	19.8 ± 0.7	0.9 ± 38.9	4.1 ± 6.3		18.9%
4	19.3 ± 11.9	0.1 ± 46.5	3.8 ± 19.5	6.5 ± 27.1	16.1%

$T = 11$

M	E_1	E_2	F_{min}/F_0
1	13.4 ± 4.3		25.0%
2	13.4 ± 5.0	1.7 ± 0.0	24.5%

$T = 7.3$

M	E_1	F_{min}/F_0
1	4.3 ± 1.5	44.5%

Next we have applied the model to the ζ series of the six 2 degree squares (Fig. 1). Due to the limited depth range of the XBT data we cannot expect to be able to separate several modes in this case. Also as can be seen from the fit in the time domain and the cross-spectral fit at station November the first mode appears to play a predominant role. We therefore restrict our model to the first mode in this case.

Since observations from more than one location are to be used $\mathbf{r} \neq 0$ and we must specify $S_1(\phi)$ in (5.5). The simplest assumption is a discrete directional distribution of $E(\mathbf{K},\omega)$ and we therefore let

$$S_1(\phi) = \delta(\phi - \phi_1) \ . \tag{6.8}$$

With these assumptions (5.6) becomes

$$A(r,z,z',\omega) = E_1\phi_1(z)\phi_1(z') \exp\{-i[\ \beta/2\omega\ \ r \sin\alpha + R_1\, r\cos(\phi_1-\alpha)]\} \tag{6.9}$$

The cross-spectra thus defined were then fit to the cross-spectra computed from the ζ fluctuations at the different locations:

$$C_*^{(s)} = C_*(r_s,\alpha_s,z_s,z'_s,\omega);\ Q_*^{(s)} = Q_*(r_s,\alpha_s,z_s,z'_s,\omega) \ .$$

The quadruple r_s, α_s, z_s, z'_s describes the locations of pairs of points (x_s, z_s), (x'_s, z_s') s again indicates the pair number.

In this case the expression to minimize from (6.4) and (6.9) is

$$F(E_1,\phi_1) = \sum_{s=1}^{S} [(C_*^{(s)} - D_{1s}\, E_1 \cos B_s)^2 + \ (Q_*^{(s)} - D_{1s}\, E_1 \sin B_s)^2] \tag{6.10}$$

where $B_s = \frac{\beta}{2\omega} r_s \sin \alpha_s + R_1 r_s \cos(\phi_1 - \alpha_s)$.

From $\frac{\partial F}{\partial E_1} = 0$ we obtain

$$E_1(\phi_1) = \frac{\sum_{s=1}^{S} D_{1s}(C_*^{(s)} \cos B_s + Q_*^{(s)} \sin B_s)}{\sum_{s=1}^{S} D^2{}_{1s}} \tag{6.11}$$

Using (6.7) and (6.11), (6.10) can be written as

$$F(\phi_1) = F_0 - \frac{\left[\sum_{s=1}^{S} D_{1s}(C_*^{(s)} \cos B_s + Q_*^{(s)} \sin B_s)\right]^2}{\sum_{s=1}^{S} D^2{}_{1s}} \tag{6.12}$$

We can see from (6.12) that minimizing F is identical to maximizing $E_1(\phi_1)$ in (6.11).

We have performed this fit for two sets of ζ series from the six 2 degree squares, referred to as schemes I and II (Fig. 1). Scheme I contains 7 isotherms (9° to 15°C) of squares 1, 2 and 3 giving a total of 21 series. Scheme II consists of 7 isotherms (9° to 15°C) of squares 1, 2, 3 and 6 and 4 isotherms (12° to 15°C) of square 5 and the 15°C isotherm of square 4, a total of 33 series. Scheme I was chosen as a sample that would best satisfy the assumption of horizontal homogeneity. Scheme II was a test which included all useable ζ series and although it may not satisfy this assumption as well as scheme I, it does have better statistical significance because of the larger number of series.

We calculated $E_1(\phi_1)$ for both schemes according to (6.11) as well as F_{min}/F_0. The results are shown in Fig. 8 for the period of 28 months. The maxima of E_1 are indicated along with the corresponding minima of $F_{\min}/F_0$. At these points the wavelength λ and the direction of propagation γ (γ positive from north to west, Fig. 7) of the respective waves are given. The maxima of E_1 along with the corresponding values of ϕ_1 and F_{min}/F_0 are given in Table 5. In addition, the appropriate wave lengths, directions of propagation, phase speed c and group speed c_g are presented.

As the next step we have made a more general assumption about the directional distribution of $E(\mathbf{k},\omega)$. Following Schott and Willebrand (1973) we let

$$S_1(\phi) = \delta_1 \cos^{2P_1}\left(\frac{\phi - \phi_1}{2}\right) \tag{6.13}$$

This means that we allow the waves to propagate in a beam centered around ϕ_1,

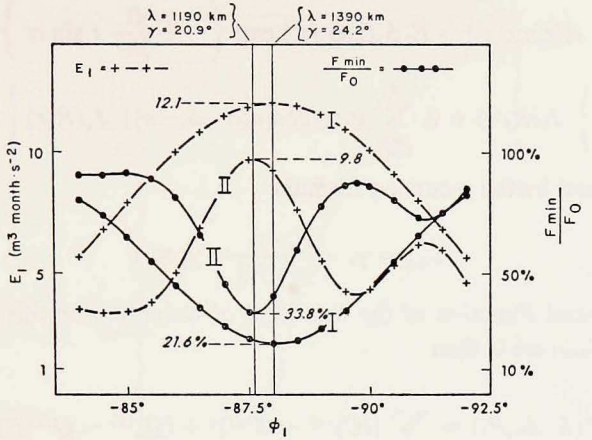

Figure 8. E_1 (ϕ_1) and $F_{\min}/F_0$ at period $T = 28$ months for schemes I and II.

the width of which is described by the angle ϵ_1 defined by $\cos^{2P_1} \epsilon_1/4 = \frac{1}{2}$ (see Fig. 7). The factor δ_1 is determined by the normalization condition (5.8). For this propagation distribution we find from (5.6)

Table 5. Results of the "δ-function" fit (with standard error).

T(months)	Scheme	$E_1(m^3 \text{month} \cdot s^{-2})$	ϕ_1	λ(km)
28	I	12.1 ± 2.9	−88.0° ± 0.8°	1390 ± 470
28	II	9.8 ± 4.8	−87.6° ± 0.5°	1190 ± 220
14	I	11.7 ± 3.0	−88.0° ± 1.8°	1500 ± 320
14	II	9.4 ± 5.1	−89.1° ± 1.1°	1670 ± 120
9.3	I	6.6 ± 3.0	−96.7° ± 5.0°	880 ± 240
9.3	II	6.5 ± 5.2	−99.4° ± 2.1°	750 ± 90
7	I	4.5 ± 2.2	−68.1° ± 10.8°	490 ± 140
7	II	4.4 ± 3.4	−66.6° ± 13.6°	480 ± 170
5.6	I	4.3 ± 1.3	−21.0° ± 13.7°	280 ± 40
5.6	II	3.5 ± 3.0	−15.6° ± 5.6°	260 ± 10

T(months)	Scheme	γ	c(cm s^{-1})	c_g(cm s^{-1})	$F_{\min}/F_0$
28	I	24.2° ± 7.5°	1.9	4.6	21.6%
28	II	20.9° ± 3.4°	1.6	4.5	33.8%
14	I	62.0° ± 20.9°	4.1	4.4	27.3%
14	II	76.4° ± 16.0°	4.6	4.4	38.2%
9.3	I	123.7° ± 18.2°	3.7	3.7	60.0%
9.3	II	132.0° ± 5.4°	3.1	3.6	61.9%
7	I	50.3° ± 8.8°	2.7	2.5	73.2%
7	II	49.2° ± 9.7°	2.6	2.5	68.1%
5.6	I	59.7° ± 1.2°	1.9	1.1	49.0%
5.6	II	60.3° ± 0.7°	1.8	1.1	70.6%

$$A(\mathbf{r},z,z',\omega) = E_1\phi_1(z)\phi_1(z') \exp\left\{ -i\frac{\beta}{2\omega} r \sin\alpha \right\} \times$$

$$\left\{ J_0(R_1 r) + 2 \sum_{v=1}^{\infty} i^v \gamma_v \cos[\nu(\alpha-\phi_1-\pi)]\ J_v(R_1 r) \right\} \tag{6.14}$$

where γ_v is defined by the recursion formula

$$\gamma_{v+1} = \gamma_v \frac{P_1-\nu}{P_1+\nu+1}\ ;\ \gamma_0 = 1 \tag{6.15}$$

and J_v is the Bessel Function of the first kind of order v. For this general case the expression to minimize is then

$$F(E_1,\phi_1,P_1) = \sum_{s=1}^{S} [(C_*^{(s)} - C^{(s)})^2 + (Q_*^{(s)} - Q^{(s)})^2] \tag{6.16}$$

where $C^{(s)}$ and $Q^{(s)}$ can be found from (6.14).

From $\dfrac{\partial F}{\partial E_1} = 0$ we get

$$E_1 = \frac{\sum_{s=1}^{S} (C_*^{(s)} c_s + Q_*^{(s)} q_s)}{\sum_{s=1}^{S} (c_s^2 + q_s^2)} \tag{6.17}$$

where $c_s = \dfrac{C^{(s)}}{E_1}$ and $q_s = \dfrac{Q^{(s)}}{E_1}$. Note that c_s and q_s are independent of E_1. From (6.16) and (6.17) we find that minimizing F (E_1, ϕ_1, P_1) is equivalent to maximizing the expression

$$G(\phi_1\, P_1) = \frac{\left[\sum_{s=1}^{S} (C_*^{(s)} c_s + Q_*^{(s)} q_s) \right]^2}{\sum_{s=1}^{S} (c_s^2 + q_s^2)} \tag{6.18}$$

This was done by tabulating G for appropriate values of ϕ_1 and P_1. In doing so the upper limit of the sum in (6.14) was replaced by

$$N = 2 + \text{entire} \begin{cases} 8R_1 r + 4.8 \text{ for } R_1 r < .87 \\ 2R_1 r + 10.0 \text{ for } R_1 r \geqq .87 \end{cases} \tag{6.19}$$

(See Murray, 1967).

The results of maximizing G in (6.18) are given in Table 6, where instead of P_1 we present the beam width ϵ_1. An example of the dependence of F_{min}/F_0 on ϵ_1 at constant ϕ_1 is shown in Fig. 9.

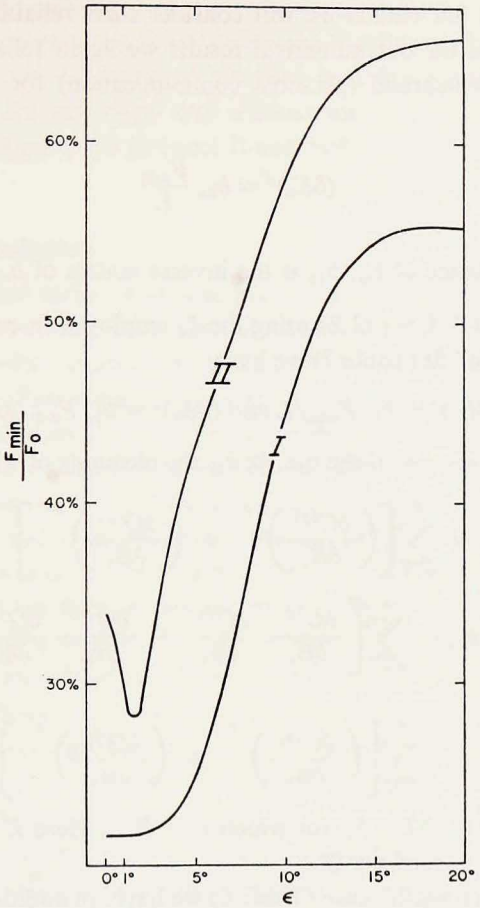

Figure 9. F_{min}/F_0 as function of ϵ_1 at period $T = 28$ months for schemes I and II.

Table 6. Result of the "finite beam width" fit (with standard error).

T(months)	Scheme	$E_1(m^3\text{month}\cdot s^{-2})$	ϕ_1	ϵ_1	F_{min}/F_0
28	I	12.1 ± 2.9	−88.0° ± 0.8°	0°	21.6%
28	II	11.8 ± 4.5	−87.6° ± 0.5°	1.5° ± 2.8°	28.2%
14	I	11.7 ± 3.0	−88.0° ± 1.8°	0°	27.3%
14	II	10.7 ± 4.9	−89.1° ± 1.2°	2.5° ± 7.4°	35.9%
9.3	I	7.9 ± 5.7	−96.7° ± 9.6°	16.8° ± 89.7°	57.9%
9.3	II	6.5 ± 5.2	−99.4° ± 2.1°	0°	61.9%
7	I	9.8 ± 3.9	−68.1° ± 360°	360° ± 360°	46.9%
7	II	9.6± 4.6	−66.6° ± 360°	360° ± 360°	58.8%
5.6	I	7.7 ± 2.1	−74.0° ± 56.0°	210° ± 304°	27.0%
5.6	II	7.9 ± 3.9	−75.0° ± 107°	230° ± 360°	58.4%

Before we discuss our results we will consider their reliability and accuracy. In calculating error bars for our numerical results we again follow Schott and Willebrand (1973) and Willebrand (personal communication) for the values of E_n. In Table 4 we have

$$(\delta E_n)^2 = b_{nn} \frac{F_{min}}{L} \tag{6.20}$$

where δE_n is the variance of E_n, b_{ik} is the inverse matrix of $a_{ik} = \sum_{s=1}^{S} D_{is} D_{ks}$ and $L = K - M$. We find K from (3.2) using the ζ_i employed in each fit and $\alpha_i = 1$.

For the "δ-function" fit (Table 5) we have

$$(\delta E_1)^2 = b_{11} F_{min}/L \text{ and } (\delta\phi_1)^2 = b_{22} F_{min}/L \ . \tag{6.21}$$

In this case b_{ik} is the inverse of the matrix a_{ik} the elements of which are

$$\begin{aligned} a_{11} &= \sum_{s=1}^{S}\left[\left(\frac{\partial C^{(s)}}{\partial E_1}\right)^2 + \left(\frac{\partial Q^{(s)}}{\partial E_1}\right)^2\right] \\ a_{12} = a_{21} &= \sum_{s=1}^{S}\left[\frac{\partial C^{(s)}}{\partial E_1}\frac{\partial C^{(s)}}{\partial \phi_1} + \frac{\partial Q^{(s)}}{\partial E_1}\frac{\partial Q^{(s)}}{\partial \phi_1}\right] \\ a_{22} &= \sum_{s=1}^{S}\left[\left(\frac{\partial C^{(s)}}{\partial \phi_1}\right)^2 + \left(\frac{\partial Q^{(s)}}{\partial \phi_1}\right)^2\right] \end{aligned} \tag{6.22}$$

evaluated at the values of E_1, ϕ_1, for which $F = F_{min}$. Here $L = K - 2$ where K is again found from the ζ_i used per fit.

For the "finite beam width" case (Table 6) we have, in addition to (6.20)

$$(\delta P_1)^2 = b_{33} F_{min}/L \ . \tag{6.23}$$

The matrix a_{ik} also has the additional elements

$$\begin{aligned} a_{31} = a_{13} &= \sum_{s=1}^{S}\left[\frac{\partial C^{(s)}}{\partial E_1}\frac{\partial C^{(s)}}{\partial P_1} + \frac{\partial Q^{(s)}}{\partial E_1}\frac{\partial Q^{(s)}}{\partial P_1}\right] \\ a_{32} = a_{23} &= \sum_{s=1}^{S}\left[\frac{\partial C^{(s)}}{\partial \phi_1}\frac{\partial C^{(s)}}{\partial P_1} + \frac{\partial Q^{(s)}}{\partial \phi_1}\frac{\partial Q^{(s)}}{\partial P_1}\right] \\ a_{33} &= \sum_{s=1}^{S}\left[\left(\frac{\partial C^{(s)}}{\partial P_1}\right)^2 + \left(\frac{\partial Q^{(s)}}{\partial P_1}\right)^2\right]. \end{aligned} \tag{6.24}$$

All elements of a_{ik} are evaluated at E_1, ϕ_1, p_1 for $F = F_{min}$.

For this case $L = K-3$. The error bars in Tables 4, 5 and 6 are at the 80% level.

To further check the reliability of the cross-spectral fit, we replaced the ζ series for both schemes with random data uniformly distributed between −25 m and +25 m and repeated the "δ-function" fit. The resulting E_1 (ϕ_1) distributions, for 28 and 14 months, did not show any distinct maxima. Also the corresponding F_{min}/F_0 values were about 96% (scheme I) and 98% (scheme II).

7. Discussion and conclusions

When analyzing time series of almost five years in length for periods between 5 and 28 months the problem of statistical significance of the results becomes a crucial one. We therefore started our analysis with a nonstatistical method: fitting in the time domain. Proceeding to statistical methods (spectral analysis, cross-spectral fits) we have seen that due to the dependence between series the large number of time series makes up for the shortness of the series only to a limited extent. The number of degrees of freedom of the composite spectrum (about 10 to 11 versus 4 for the individual spectra) reveals that in terms of statistical independence our ζ series contain about three independent data sets. This is consistent with our finding that the fluctuations are mainly due to long first-order waves. A meaningful cross-spectral fit of such waves to data requires the different ζ series to be sufficiently dependent. Moreover, they have to cover adequately the region under consideration. These requirements determined the number of series we have taken from the XBT and hydrographic data. A smaller number would have violated the necessity of adequate coverage with respect to space; a larger number would not have given any additional insight.

The high degree of dependence of our ζ series leads to reduced statistical significance of our results. High statistical significance for a cross-spectral fit can only be achieved if the series are long compared to the periods in question, i.e. of the order of 100 years in our case. Since this condition was not met the standard errors of our numerical results are rather large. They are, however, small enough to permit meaningful conclusions.

The dependence between series is strongest at weather station November since only one location is involved. Only the first mode can be determined with any accuracy; the energies of the other modes cannot be shown to be significantly different from zero. The numbers for F_{min}/F_0 show that for periods of 22 and 11 months a large portion of the fluctuations can be described by the first mode. As can be seen in Schott (1974) a figure below 20% for F_{min}/F_0 is rare in mode fitting.

The application of the model to the XBT data from squares 1 through 6 is, of course, a more exacting test since it involves to a much higher degree the dispersion relationship of the waves. Tables 5 and 6 show that at periods of 14 and 28 months the best fit waves have a well defined direction of propagation. The results for scheme I are in reasonable agreement with those for $M = 1$ in Table 4. The fit is

somewhat poorer for scheme II, however, they are not inconsistent with those for scheme I. At periods 9.3, 7, and 5.6 months the "δ-function" fit is poor for both schemes I and II. Using the "finite beam width" fit the F_{min}/F_0 values are made smaller than those for the "δ-function fit", in some cases (scheme I, 7 and 5.6 months) substantially smaller. At 7 months the results of the "finite beam width" fit agree with the results from the weather station (Table 4).

The standard error in Table 6 is largest for ϵ_1. This also follows the results of Schott (1974) for internal gravity waves. The ϵ_1 values for wave periods 7 and 5.6 months indicate that the angular range of propagation directions opens up for these periods to isotropic propagation in the western half plane. The ϵ_1 values are not significant statistically. The reduction of F_{min}/F_0 value, however, through the "finite beam width" fit to the values of Table 4 which represent the integrated contribution from all propagation directions, supports the idea that the ϵ_1 values are more accurate than the error bars indicate. Based on the consistency of the results from different data sets (hydrographic data from the weather station, XBT data from squares 1 through 6) we believe that the same is true for all our results. In summary, of our results the most significant and important are those for the 14 and 28 month periods. Waves at these periods propagate with "δ-function" directional distribution in the north-west quadrant. They have wave lengths on the order of 1200 to 1700 km. Their group velocities are directed westward with magnitudes of about 4.5 cm s^{-1}.

Acknowledgments. We wish to thank Dr. H. G. Loomis for making his spectral routines available to us and for his continuing assistance in their use. We further acknowledge the assistance of Mr. M. A. Sklarz who allowed us to use his program for the computation of the internal wave modes and helped us to apply it. Dr. J. Willebrand has given us substantial help in determining the confidence limits of our numerical results. This help is gratefully acknowledged.

This research has been supported by the Office of Naval Research under the North Pacific Experiment of the International Decade of Ocean Exploration; this support is gratefully acknowledged. This paper is Contribution No. 760 of the Hawaii Institute of Geophysics.

REFERENCES

Bernstein, R. A., and W. B. White. 1974. Time and length scales of baroclinic eddies in the Central North Pacific Ocean. J. Phys. Oceanogr., *4*, 613–624.

Emery, W. J. 1975. The role of vertical motion in the heat budget of the upper ocean. Hawaii Institute of Geophysics Rep. *HIG–75–3*, 81 pp.

Husby, D. M. 1968. Oceanographic observations North Pacific Ocean station November, July 1966–February 1967. U.S.C.G. Report No. 18, United States Coast Guard, Washington, D.C.

Murray, W. 1967. Computation of Bessel functions. National Physical Laboratory, Teddington, England.

Preisendorfer, R. W., J. C. Larsen, and M. A. Sklarz. 1974. Electromagnetic fields induced by plane–parallel internal and surface ocean waves. Hawaii Institute of Geophysics Rep. *HIG–74–7*, 306 pp.

Schott, F. 1974. Ueber die raumzeitliche Struktur von Stromschwankungen im Meer unter besonderer Beruecksichtigung barokliner Gezeiten. Habilitationsschrift, Kiel.

Schott, F. and J. Willebrand. 1973. On the determination of internal wave directional spectra from moored instruments. J. Mar. Res., *31*, 116–134.

Received: *7 September, 1975;* revised: *14 April, 1976.*